Safont Armero, G.; Salazar Afanador, A.; Vergara Domínguez, L.; Vidal Maciá, AM.; Gonzalez, A. (2013). Assessment of historic structures based on GPR, ultrasound, and impact-echo data fusion. Key Engineering Materials. 569-570:1210-1217. doi:10.4028/www.scientific.net/KEM.569-570.1210.

Assessment of historic structures based on GPR, ultrasound, and impact-echo data fusion

Gonzalo Safont[1,a], Addisson Salazar[1,b] and Luis Vergara[1,c] Antonio Vidal[2], Alberto Gonzalez[1]

Universitat Politècnica de Valencia

[1]Institute of Telecommunications and Multimedia Applications

[2]Department of Information Systems and Computation

Camino de Vera s/n, 46022, Valencia, Spain

[a]gonsaar@upvnet.upv.es, [b]asalazar@dcom.upv.es, [c]lvergara@dcom.upv.es

Keywords: data fusion, non-destructive testing, structure assessment, material defect detection.

Abstract. This paper presents a method for assessment of historic structures based on the fusion of data from ground-penetrating radar (GPR), ultrasound, and impact-echo testing. The method consists of the following steps: measuring, feature extraction, fusion, representation, and evaluation. The employed techniques for an application in scale models of historical walls are described. Thus, experimental deployment; signal feature processing; fusion operators (including order statistics digital filters); 2D non-destructive testing images, and figures of merits of the fused results are explained in detail. The deformation of different imperfections in the material structure related to the application of weight load increments applied on the wall is analyzed by using different kinds of fusion configurations.

Introduction

The principal objective of this paper is to provide an approach for non-destructive testing (NDT) based on impact-echo, ultrasound and ground-penetrating radar (GPR) signal processing for diagnoses of historical walls. Common materials employed in heritage buildings are stone, mortar and brick. This kind of constructions resists well the pass of the time; nonetheless, degradation processes are inevitable and difficulties arise for measuring its degree of degradation. The degradation processes affect both structural (cracks, fissures, detachments, displacements, etc.~~...~~) and aesthetic (dirt, crusts, efflorescence, etc.~~...~~) characteristics of the historical buildings. Among the main pathologies that cause building breakdown are humidity damages caused by capillarity ascent, breeze or high humidity environments, successive freeze-thaw cycles that result in crystallization, and broken mortar joints. At present, to deal with structural evaluation, it is usual to use destructive testing by means of the extraction and characterization of ~~tubes~~ cylindrical samples from the material that are characterized using classical morphological and physiochemical analyses. Thus, considering heritage value preservation, NDT is being increasingly applied in pathological and structural diagnoses of historical buildings.

In this paper, we present results of testing two scale models of historic ashlar masonry walls using through-transmission ultrasounds (two transducers, an emitter and a receiver each one located at opposite sides of the wall) and pulse-echo GPR (an antenna used as emitter and receiver located at one side of the wall). The walls were built with travertine ashlars from Godella's quarry in Spain and the dimension of the ashlars was 41x31x20.5cm; a picture of one of the walls is shown in Figure 1~~Figure 1~~. The final dimension of the two walls was 287cm x 220 cm x 20.5 cm (length, height and thickness). Impoverished mortar with a low compression resistance (<4MPa) was used as binding material. ~~One of the walls~~ The first wall was homogeneous, and the second one was

mechanized ~~including~~ to include artificial defects (two drill holes, a vertical flaw and a crack or nook filled with mortar, see Figure 2~~Figure 2~~).

Figure 1. Ashlar inhomogeneous masonry wall.

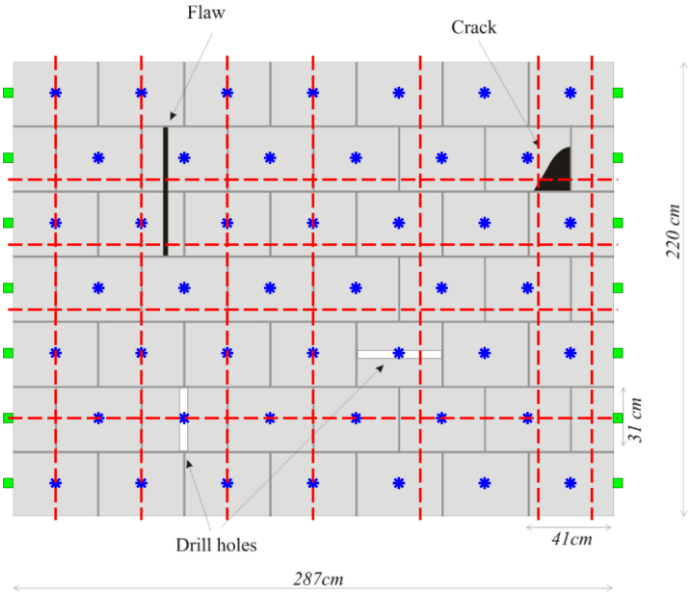

Figure 2. Defect and measurement outline.

Capture positions are presented in Figure 2~~Figure 2~~ for the three considered NDT methods. Ultrasound measurements were taken in the 42 positions indicated by blue asterisks. Radar signals were collected using a survey cart with encoder through the 11 trajectories depicted by red dashed lines. Finally, impact-echo signals were captured at 14 positions in the sides of the wall, as shown by green squares (impacts were generated at each one of the capture positions). In order to evaluate the sensitivity of the NDT methods to the tensional states of the walls, the walls were fit in a hydraulic press and loaded with 10 t~~Tn~~, 50 t~~Tn~~ and 80 t~~Tn~~.

Impact-echo, ultrasonic and GPR inspection are based on mechanical, mechanical and electromagnetic waves, respectively. These waves propagate inside the material structure and its response is measured by signals that contain the reflections produced by the material grain microstructure plus the echoes caused by the ~~in homogeneities~~inhomogeneities inside the material

[1, 2]. Signal processing allows extraction of information for characterization of the propagation medium and for detecting material ~~in homogeneities~~inhomogeneities [3]. In this paper, we present results in detection of defects in the wall scale models by impact-echo, ultrasounds and GPR separately (each one in a separate section~~Section 2, 3 and 4~~) and enhanced results ~~(Section 5)~~ obtained by fusing all three results. Data fusion is a new method that is progressively finding more applications in NDT, such as fusion of X-ray and ultrasound images in welds, and infrared thermography imagery in nuclear applications. The fusion methods employed have been based on classification systems and recently data fusion was done using possibility theory and fuzzy sets [4]. The fusion method presented here combines impact-echo, ultrasound and radar images estimated from the propagation velocity and signal power. From the original measurements, 2D images are formed using interpolation and morphological transformations; after fusion, the fused image is filtered using an order statistical digital filter.

Ultrasonic tomography

NDT by ultrasounds is a very useful technique that has been applied in several fields such as construction, food, and biomedicine. Only through-transmission was considered. In this technique, the ultrasound pulse is injected in the inspected material through an emitter, and the response of the material structure is received on a separate sensor on the other side of the material under test. The measured signal can contain echoes produced from discontinuities, inhomogeneities, borders of the material, plus material grain noise (superimposition of many small echoes due to the material microstructure). All of this information can be used for quality control and characterization of materials since physical properties of the material, such as porosity and density, have a definite influence on the propagation of the ultrasound [1].

An ultrasonic signal (A-Scan) was measured for each spatial position described in Figure 2~~Figure 2~~. The following parameters were extracted from ultrasonic signals: propagation velocity (V), signal power (P) and maximum frequency (f_{max}), see Table 1. The temporal window used for their estimation begins at 30µs and finish at 100µs. Once the ultrasonic parameters were extracted for each, a 2D image usually called B-Scan can be obtained. In this ultrasonic image or tomography X axis is associated to the length and Y axis is associated to height of the wall. The color of the image represents the value of the ultrasonic parameter. The variation of the color represents the variation of the ultrasonic parameters that can be related to the shape and spatial position of the defects. In order to obtain realistic visualization (smoothed eliminating sharp edges) of the wall tomography, a classical linear interpolation algorithm called ordinary Kriging was applied [5].

Con formato: Subíndice

Several tomographies were estimated for each of the ultrasonic parameters and load steps. The variations of the tomography values that were expecting to associate with defects, were masked by variations of the own material and measurement variance. Thus, differential tomographies were obtained by subtracting tomographies corresponding to different load steps (e.g., subtracting 10Tn tomography from 50Tn tomography). By this way, the variations between the ultrasonic parameter and the variations of the load were compared (ultrasonic parameters are sensitive to tensional state; velocity and signal power suffer an increment with load whereas central frequency is kept constant). Figure 3~~Figure 3~~ shows a differential 50Tn-10Tn tomography, where some defects are detected. The rationale is that ultrasonic dependence with load is different between sound and unsound zones and ultrasonic parameters suffer different percentage of variation, as reflected in Figure 3~~Figure 3~~. The vertical flaw and horizontal drill hole were not detected because the load was not so high to suppose an important variation of the ultrasonic parameter, in this case, velocity. The crack is detected and it is possible to note how this defect affects adjacent ashlars.

Con formato: Sangría: Primera línea: 0,5 cm, Espacio Después: 6 pto

Table 1. Parameters extracted from the ultrasonic signals.

$V = \frac{Distance}{\text{Time of flight}} = \frac{d}{\Delta t}$	$f_{\max}[Hz] = \underset{f}{\max}\left\{X_{N_{samples}}(f)\right\}$
$P = \frac{\sum \lvert x[n] \rvert^2}{50 N_{Samples}}$	$X_{N_{samples}}(f) = TF\left\{x_{N_{samples}}(n)\right\}$
	$x_{N_{samples}}(n) \rightarrow N_{samples}\ \text{truncated from}\ x(n)$

Impact-echo tomography

In the impact-echo technique, a material is impacted with a hammer, which produces a response that is sensed by a mono- or multi-sensor system that is located on the surface of the material. The impact-echo signals contain backscattering from grain microstructure as well as information about flaws in the inspected material. The physical phenomenon of impact-echo corresponds to wave propagation in solids. When a disturbance is applied suddenly at a point on the surface of a solid, the disturbance propagates through the solid as three different types of waves: P-wave (normal stress), S-wave (shear stress), and R-wave (surface or Rayleigh) [6]. After a transient period in which the first waves arrive, wave propagation becomes stationary in resonant modes that vary depending on the defects inside the material.

The impact-echo signals were captured at 14 locations in the sides of the wall, as described in Figure 2~~Figure 2~~. There were a total of 14 impacts, each one located besides one of the receivers, capturing a total of 196 signals for each load step. Propagation velocity (V) was estimated for each signal. The temporal window used for their estimation begins at time 0 and finishes at 3600 µs. These 1D signals are then interpolated to form a 2D tomography; the interpolation was performed by using an algorithm based on radial basis function neural networks (RBFNN, [7]). The axes of this interpolation were identical to those of the ultrasound tomography, with color indicating the value of the calculated parameter (in this case, propagation velocity).

A different propagation velocity tomography was obtained for each load step. Differential tomographies were obtained by subtracting tomographies from different load steps, following the same process used for ultrasound tomographies. ~~Figure 5~~ shows the differential 50Tn-10Tn tomography. The results show a lower resolution that ultrasound tomography, as expected from the density of capture sensors, and no defect was located. Propagation velocity is shown to be higher at the right side of the wall, near the crack, and decreases gradually until a minimum value at the bottom left corner of the wall.

Código de campo cambiado

GPR tomography

Ground Penetrating Radar (GPR) is a Non-Destructive Evaluation (NDE) method that uses electromagnetic waves to study the composition of a material. The GPR equipment transmits pulses of radio waves through the material structure. Afterwards, the response of the material is measured by signals that contain the reflections produced by the microstructure plus the echoes caused by the inhomogeneities inside the material [8]. The principal goal of the GPR signal processing consists of characterizes the propagation medium and then subtracting it from the measured signals in order to detect the material inhomogeneities. GPR has been used in several applications such as detection of non-metallic land mines; concrete and rebar imaging and inspection; and a few references in historic buildings NDT [9].

Processing of GPR signals included three common processing steps: background signal removal, depth resolution enhancing and Kirchoff migration. The result of this processing is a radargram, which is an image (also called B-Scan) that represents values of the measured signal (in this case we used signal power) at different depths of the material through the points of a trajectory (defined in Figure 2~~Figure 2~~). The objective of the several processing steps was to highlight the zones in the

radargram where the inhomogeneities were located. Thus, envelope estimation and automatic gain control were also implemented for data interpretation and to enhance the image contrast.

A tomography was obtained by merging the 11 radargrams obtained for each of the GPR trajectories. This image was cleaned applying morphological operations using disk-shaped structuring element with a radius of 5 pixels and thresholding power values to .7 of the maximum. This last guarantees only high reflections to be represented and filtering spurious reflections. As in the ultrasound tomography processing, an interpolation algorithm was used to generate a smoothed tomography. Figure 5~~Figure 4~~ shows the GPR tomography obtained for the inhomogeneous wall at 50Tn load step. The high reflection produced by the flaw and the power decrease caused by the crack are depicted. These defects affect wave propagation travelling depending on its shape in two different ways, in the case of the crack; the propagated waves have to surround the defects and therefore their energy decreases. In the case of the flaw, multiple reflections and diffraction with the defect borders arise.

~~Table 1.~~ ~~Parameters extracted from the ultrasonic signals.~~

$V = \frac{Distance}{\text{Time of flight}} = \frac{d}{\Delta t}$	$P = \frac{\sum \lvert x[n] \rvert^2}{50 N_{Samples}}$
$P = \frac{\sum \lvert x[n] \rvert^2}{50 N_{Samples}}$	$f_{\max}[Hz] = \underbrace{\max}_{f} \{X_{N_{samples}}(f)\}$
	$X_{N_{samples}}(f) = TF\{x_{N_{samples}}(n)\}$
	$x_{N_{samples}}(n) \rightarrow N_{samples}\ \text{truncated from}\ x(n)$

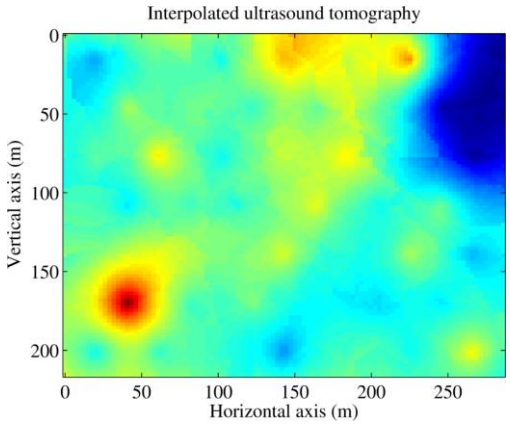

Figure 3. Differential ultrasound tomography.

Con formato: TTP Paragraph (1st), Sangría: Primera línea: 0,5 cm

Con formato: TTP Paragraph (1st)

Con formato: TTP Paragraph (1st), Ajustar espacio entre texto latino y asiático, Ajustar espacio entre texto asiático y números

Con formato: TTP Paragraph (1st), Ajustar espacio entre texto latino y asiático, Ajustar espacio entre texto asiático y números

Código de campo cambiado

Con formato: TTP Paragraph (1st)

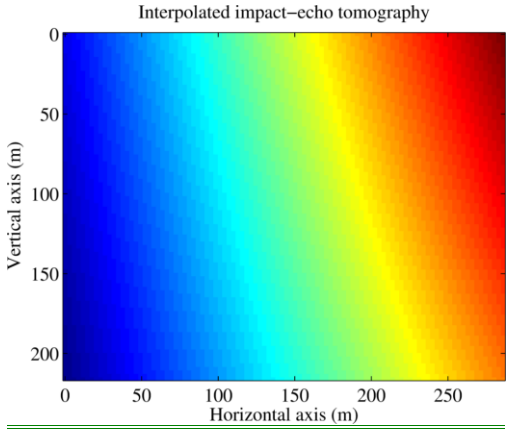

Figure 4~~5~~. Differential impact-echo tomography.

Con formato: Epígrafe

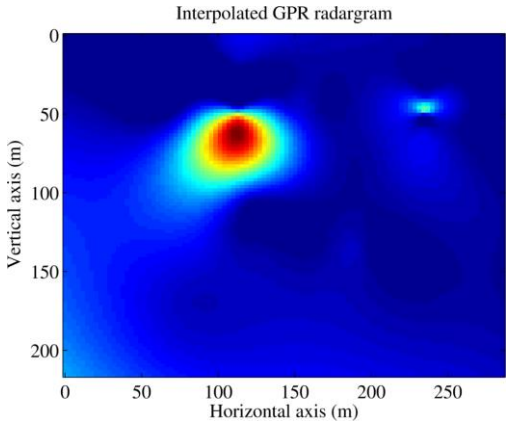

Figure 5~~4~~. GPR tomography.

Con formato: Epígrafe

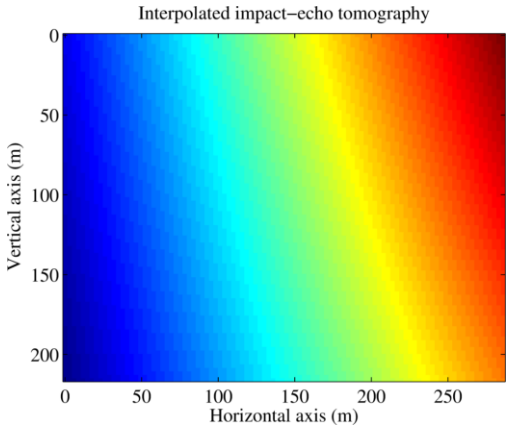

~~Figure 5. Differential impact-echo tomography.~~

Results ~~and Conclusion~~

Figure 6~~Figure 6~~ and Figure 7~~Figure 7~~~~¡Error! No se encuentra el origen de la referencia.~~ represent fused tomographies obtained from the separate results for impact-echo, ultrasound and GPR B-scans explained in previous sections. The operators for combining the tomographies were the product and the sample mean for Figure 6~~Figure 6~~ and Figure 7, respectively. After fusion, the fused images were filtered using a median filter.

Figure 6~~Figure 6~~.a and Figure 7.a show the results from a previous work that only considers ultrasound and GPR tomographies [10]. Figure 6~~Figure 6~~.b and Figure 7.b add the information from the impact-echo tomography, improving the fused result. In both Figures, the addition of impact-echo information results in lower false alarms and a better localization of the flaw in the upper left area of the wall. The best result is Figure 7.b, the sample mean of impact-echo, ultrasound and GPR tomographies, since three of the four defects are detected and their size is nearest to the truth.

To quantify the performance of the fusion procedure, the Equal Error Rate (EER) was calculated for each tomography. For this, each tomography was thresholded to obtain a detection image. These detection images are then compared with the supposed distribution of the defects: pixels within a certain range (5 cm) of a defect are correct if they were detected, while pixels further from this range are correct if they were not detected. The threshold is changed until the false alarm rate is equal to one minus the detection rate; this common value is the EER. The lower the EER, the better the detection is. ~~Table 1~~ shows the calculated EER values: their values confirm the increase in performance obtained by considering fusion algorithms and the increase in performance by considering all three tomographies, further supporting our results.

~~Table 1. EER values for the tomographies shown in this paper.~~

Table 2. EER values for the tomographies shown in this paper.

Tomography	Ultrasound (Figure 3~~Figure 3~~)	GPR (Figure 5~~Figure 4~~)	Impact-echo (~~Figure 5~~)	Product (Figure 6~~Figure 6~~.a)	Product (Figure 6~~Figure 6~~.b)	Mean (Figure 7.a)	Mean (Figure 7.b)
EER value [%]	43.11	50.24	52.57	35.81	26.71	38.12	25.95

Conclusion

We observe that the different fusion methods produce different results. An explanation for that may be done in the framework of optimal estimation theory. Thus we may consider that the final goal of the problem is to estimate a parameter, associated to every point in the image, represented by the amplitude value of every pixel. This parameter is supposed to change (normally increasing) due to the presence of a defect. The values measured by each separate method may be considered "observations" from which the parameter is to be estimated. In Bayes estimation theory [11], the parameter and the observations are considered random variables having some marginal and joint distributions, and the optimum estimator corresponds to the one minimizing some cost function. It is, for example, well-known, that the minimum mean-square error (MMSE) estimator is given by the expected value of the parameter conditioned to the observations. In general, this conditioned expected value is a nonlinear function of the observations, but if the marginal and joint distributions of the parameters and the observations are Gaussian the optimum estimator of the parameter is a linear combination of the observations. Actually, if the observations are uncorrelated and have equal cross-correlation to the parameter, the optimum estimator is just the sample mean of the observation, which is one the fusion method that we have implemented.

Following a similar interpretation, the fusion implementing the product is optimum when the marginal and joint distributions of the parameter and the observation are log-normal (equivalent to a linear combination after taking logarithms). In a general case the appropriate non-linear function will depend on the underlying distributions. Among them those ones based in order statistics [12] are very popular. Thus, we have experimented also with the fusion based in selecting the maximum

Con formato: Inglés (Estados Unidos)
Con formato: Inglés (Estados Unidos)
Código de campo cambiado
Con formato: Inglés (Estados Unidos)
Código de campo cambiado
Con formato: Inglés (Estados Unidos)
Código de campo cambiado
Con formato: Inglés (Estados Unidos)
Código de campo cambiado
Código de campo cambiado
Con formato: Sangría: Primera línea: 0 cm

value of the two observations, although other methods could be tried. Considering the obtained results it seems that the Gaussianity and uncorrelation assumptions are reasonable in our case, as the best performance has been obtained with the fusion implementing the sample mean of the two images.

The real-time processing of all the data from the experiments would demand high computational capabilities. To deal with this problem, we are currently investigating in the parallelization of the algorithms in order to implement them in multiprocessor structures.

a) b)

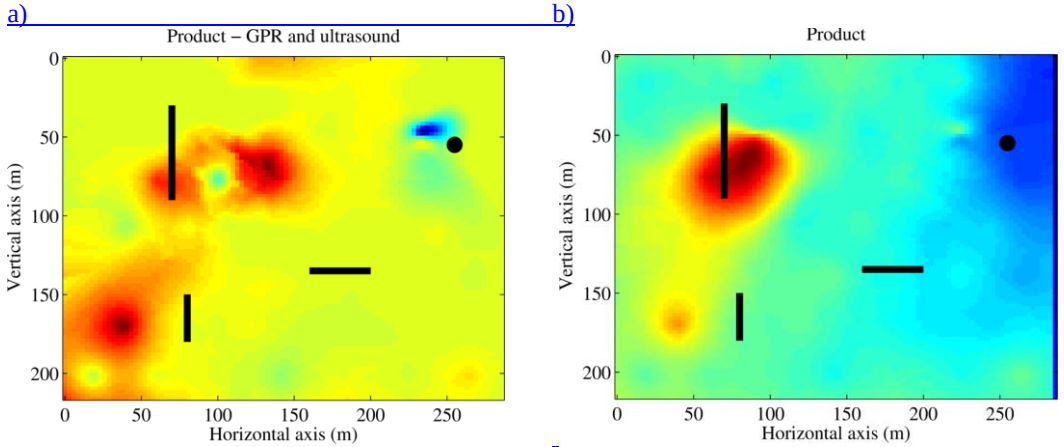

Figure 6. Fused tomography by product.

a) b)

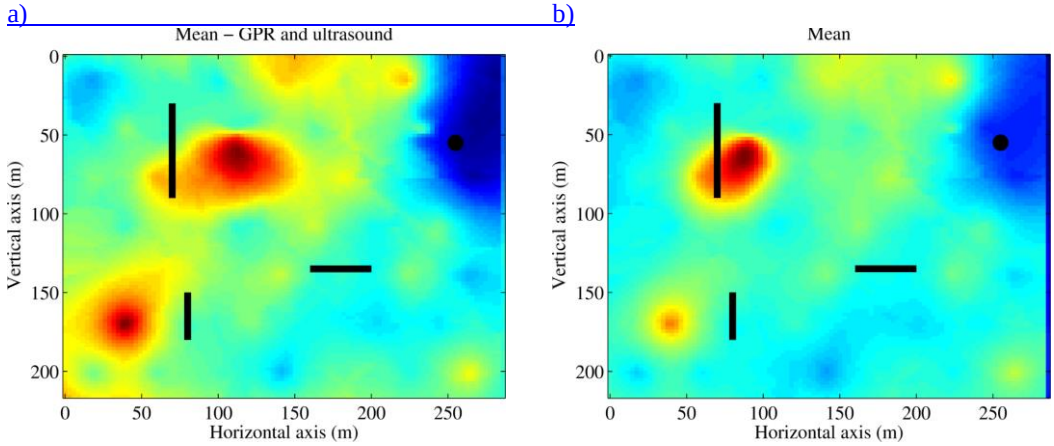

Figure 7. Fused tomography by sample mean.

~~Conclusion~~

~~We observe that the different fusion methods produce different results. An explanation for that may be done in the framework of optimal estimation theory. Thus we may consider that the final goal of the problem is to estimate a parameter, associated to every point in the image, represented by the amplitude value of every pixel. This parameter is supposed to change (normally increasing) due to the presence of a defect. The values measured by each separate method may be considered "observations" from which the parameter is to be estimated. In Bayes estimation theory [11], the parameter and the observations are considered random variables having some marginal and joint distributions, and the optimum estimator corresponds to the one minimizing some cost function. It~~

Con formato: Sangría: Primera línea: 0 cm

Con formato: Sangría: Primera línea: 0 cm

Con formato: Epígrafe

Con formato: TTP Section Heading

Código de campo cambiado

~~is, for example, well known, that the minimum mean square error (MMSE) estimator is given by the expected value of the parameter conditioned to the observations. In general, this conditioned expected value is a nonlinear function of the observations, but if the marginal and joint distributions of the parameters and the observations are Gaussian the optimum estimator of the parameter is a linear combination of the observations. Actually, if the observations are uncorrelated and have equal cross-correlation to the parameter, the optimum estimator is just the sample mean of the observation, which is one the fusion method that we have implemented.~~

~~Following a similar interpretation, the fusion implementing the product is optimum when the marginal and joint distributions of the parameter and the observation are log normal (equivalent to a linear combination after taking logarithms). In a general case the appropriate non linear function will depend on the underlying distributions. Among them those ones based in order statistics [12] are very popular. Thus, we have experimented also with the fusion based in selecting the maximum value of the two observations, although other methods could be tried. Considering the obtained results it seems that the Gaussianity and uncorrelation assumptions are reasonable in our case, as the best performance has been obtained with the fusion implementing the sample mean of the two images.~~

~~The real time processing of all the data from the experiments would demand high computational capabilities. To deal with this problem, we are currently investigating in the parallelization of the algorithms in order to implement them in multiprocessor structures.~~

Acknowledgment

This work has been supported by Generalitat Valenciana under grants PROMETEO/2010/040 and ISIC/2012/006; and Spanish Administration and European Union FEDER Programme under grant TEC2011-23403 01/01/2012.

References

[1] J.D. Cheeke, Fundamentals and Applications of Ultrasonic Waves, CRC Press, 2002.

[2] A. Salazar and L. Vergara, ICA Mixtures Applied to Ultrasonic Nondestructive Classification of Archaeological Ceramics, Eurasip Journal on Advances in Signal Processing, 2010. doi:10.1155/2010/125201, 2010.

[3] A. Salazar, L. Vergara and R. Llinares, Learning Material Defect Patterns by Separating Mixtures of Independent Component Analyzers from NDT Sonic Signals, Mechan. Systems and Signal Proc. 24 (2010) 1870-1886.

[4] M.-A. Ploix, V. Garnier, D. Breysse and Moysan, NDE data fusion to improve the evaluation of concrete structures, NDT&E International 44 (2011) 442-448

[5] A.G. Journel and Ch.J. Huijbregts, Mining Geostatistics, The Blackburn Press, 2004.

[6] N.J. Carino, The Impact-Echo Method: an Overview, Structures Congress and Exposition, (2001), 1–18, Washington D.C., USA.

[7] V. Albert, J. Gosalbez, A. Salazar, R. Fernandez, and J.V. Fuente, Evaluación no destructiva de materiales usando métodos de reconstrucción tomográfica basados en redes neuronales de funciones de base radial, in Congreso Nacional de Ensayos no Destructivos (2011), 49-58, Valencia, Spain.

[8] J. M. Reynolds, An Introduction to Applied and Environmental Geophysics, Wiley, 1997.

[9] C. Maierhofer, S. Leipold, Radar investigation of masonry structures, NDT&E International 34 (2001), 139-147.

[10] A. Salazar, J. Gosalbez, G. Safont, and L. Vergara, Data fusion of ultrasound and GPR signals for analysis of historic walls, IOP Conference Series: Materials Science and Engineering 42 (2012), doi:10.1088/1757-899X/42/1/012008.

[11] S.M. Kay, Fundamentals of Statistical Signal Processing, Estimation Theory (vol. 1), Prentice Hall, 1993.

[12] I. Pitas I and A.N. Venetsanopoulos, Nonlinear Digital Filters, Kluwer Academic Publisher, 1990.